Larhyss Journal, ISSN 1112-3680, n°49, Mars 2022, pp. 85-122

RECTANGULAR BROAD-CRESTED FLOW METER WITH LATERAL CONTRACTION – THEORY AND EXPERIMENT

ACHOUR B.[1]*, AMARA L.[2]

[1] Professor, Research laboratory in subterranean and surface hydraulics (LARHYSS), University of Biskra, Algeria
[2] Associate Professor, Department of Civil Engineering and Hydraulics, Faculty of Science and Technology, University of Jijel, Algeria

[(*)] *bachir.achour@larhyss.net*

Research Article – Available at http://larhyss.net/ojs/index.php/larhyss/index

Received November 7, 2021, Received in revised form March 2, 2022, Accepted March 5, 2022

ABSTRACT

An in-depth theoretical and experimental study is carried out on a semi-modular device for measuring flow in open channels, in the current instance a rectangular open-channel of width *B*. The device is provided with both a crest height *P* and a lateral contraction forming a gorge of opening width *b* extending over the entire length *L* of the apparatus. This is chosen so as to ensure in all cases the appearance of a control section inside the gorge. This is the prerequisite condition for the correct functioning of the apparatus as a flow measuring device. The flow undergoes the double effect of a lateral and vertical contraction which is reflected in the following dimensionless parameters $\beta = b/B$ and $P^* = P/h_1$ where h_1 is the upstream flow depth counted over the crest height. It is shown that these two parameters can be grouped together in a single ψ variable such that $\psi = \beta/(1+P^*)$ varying in the range $]0;1[$.

The main objective of the theoretical study is to derive the stage-discharge relationship $(Q - h_1)$ and therefore that of the discharge coefficient C_d of the device. This ultimate goal is comfortably achieved based on both the momentum theorem and the energy equation, after having made certain fully justified simplifying assumptions.

The theoretical stage-discharge relationship thus obtained is consistent with semi-modular devices since the flow rate *Q* depends both on the geometric characteristics of the device and on the upstream depth h_1. Regarding the derived theoretical relationship governing the discharge coefficient, it explicitly indicates the dependence of C_d with

respect to the dimensionless parameter ψ exclusively, i.e. β and P^* parameters, which is predicted by dimensional analysis.

The theoretical discharge coefficient relationship is subjected to an experimental program as intense as it is strict. The objective is either to validate this relationship or to correct it for the effect of a correction factor if the theoretical and experimental values present some deviations.

No less than 240 measurement points are collected during tests carried out on thirteen devices with different geometric characteristics. The 240 experimental and theoretical values of the discharge coefficient are compared with each other revealing a near perfect agreement since the ratio $C_{d,Exp}/C_{d,Th}$ is extremely close to unity. This high-quality result suggests that the theoretical relationship governing the discharge coefficient can be used with confidence in its current form without undergoing any correction. Therefore, it is quite obvious to conclude that the theoretical relationship of the flow rate Q is also reliable and does not require any adjustment or correction.

Keywords: Weir, discharge, flow measurement, rectangular broad-crested weir, Theory, Experiment, discharge coefficient.

INTRODUCTION

The measurement of the flow carried by a channel of given shape is often encountered in the practice of the hydraulic engineer. There are currently many flow measurement means and each of them has its own features, drawbacks and advantages. Whether the flow takes place in a pipe or in a free surface channel, the means of measuring flow differ (Bazin, 1898: Lenz, 1943; De Coursey and Blanchard, 1970; Rehbock, 1929; SIA, 1926; Ramponi, 1949; Hager, 1986; Achour et al., 2003).

Flow metering encompasses both conventional flow measurement devices using free overspill flow and for which the downstream head is low, as well as those relying on the ability of the hydraulic jump to raise the downstream water level. The first are designated by weirs provided with a crest height, while the second are called jump flow meters.

Weirs are devices that utilize free flow over a vertical thin sill placed across the flow in a given cross-section of the channel, most often perpendicular to the longitudinal axis of the flow. They are called weirs and are based on a vertical contraction of the flow due to the presence of the crest height. This sill may have a rectangular, triangular, trapezoidal or circular notch. The flow carried by the channel is then determined by a simple point gauge reading of the upstream body of water above the crest of the weir as well as by the characteristics of the channel and of the measuring device.

The thin-walled, non-lateral contraction weir is defined by its simple geometry represented by a vertical thin-walled sill. They are well-known in the literature as "suppressed weirs". This type of weir is one of the oldest, since the first research on this

device is due to Poleny in the 18th century more precisely in 1717 (SIA, 1926). The results could lead to the establishment of the relationship between the water level h of the flow above the crest and the unit flow rate $q = Q / B$, where Q and B represent respectively the discharge and the width of the rectangular channel in which the device is inserted. This relationship is well known in the literature as the "stage-discharge" relationship. For this type of weir, it has been shown theoretically that the discharge coefficient is of the order of 0.577, or exactly $1/\sqrt{3}$. However, Poleny's observations indicate that the discharge coefficient is equal to 0.64, which leads concluding to a deviation of about 11%. This difference was attributed by Boussinesq (1877) to the effect of the curvature of the liquid streamlines crossing the crest of the weir. This curvature plays a significant role and the increase in value of the discharge coefficient is mainly due to its effect. Several discharge coefficient relationships have been proposed in the past for this type of weir, the most important of which are those of Bazin (1898), Rehbock (1929), SIA (1924), Kindsvater-Carter (1957), and Sarginson (1972).

In the Sarginson relationship, there is a parameter, noted W, which represents the Weber number. On the other hand, one may observe that all the discharge relationships, with the exception of the Kindsvater-Carter formula, contain three terms: i) a constant whose mean value is of the order of 0.61, ii) a term that takes into account the effect of surface tension and proportional to $1/h$ where h is expressed in meters. This term is found, through the Weber number, in Sarginson's relationship iii) a term which takes into account the effect of the approach flow velocity through the h/P ratio where P is the crest height. When $h / P << 1$, the effect of the approach flow velocity is weak and can be then neglected. This configuration in fact corresponds either to high crest heights P or to shallow upstream depths of the flow above the crest.

The most widely accepted unit discharge relationship today is the second version of Rehbock's formula (1929). The unit discharge is expressed both as a function of the depth of the flow h above the crest of the weir and the ratio h / P. In this relation, h is expressed in meters. The relation is applicable for $h / P < 0.5$. The precision obtained on the flow measurement varies between 0.1 and 0.2%, provided that the geometry of the weir is respected, and that the downstream liquid nappe is completely aerated.

As for the jump flow meters, these are devices presented in the form of a more or less long channel and which have a local reduction of the section or a minimum section. This reduction in the section is considered as a singularity and depending on the type of flow meter; it can be long or extremely small and can be characterized by a gradual or abrupt geometric variation. The shape of the cross section of the singularity can be arbitrarily chosen, but it is recommended that it be simple in order to avoid difficulties in its implementation. The bottom of the gauge channel may be horizontal or may have discontinuities. Some flow meters are characterized by a flat horizontal bottom and its section undergoes a gradual variation which results in a lateral contraction to a minimum section. They can also be characterized by an elevation of the bottom which results in an overhanging sill in the minimum contracted section. Finally, they can also be characterized by three sections which form a broken line. The sections located upstream

and downstream of the canal are horizontal, while the intermediate section is slightly inclined.

The flat-bottom geometry has certain advantages over others, because it causes a minimum of head losses and allows easy evacuation of sediments which could accumulate in the presence of a sill which would in effect operate as a barrier. These devices are said to be self-cleaning because the solid sediments which accumulate at the bottom of the canal or the small debris which float on the surface of the water are easily evacuated by the flow downstream of the canal. These types of gauges are said "hydraulic jump flow meters" because they causes in their downstream part a hydraulic jump by transformation of the supercritical flow, immediately downstream of the contracted section, into a subcritical flow in the flared downstream part of the channel.

The best known hydraulic jump flowmeter is the Parshall (Bos, 1976; Achour et al., 2003). It has a converging section that ends with a narrowed section called a throat, followed by a negative step. This is extended by a short ascending section constituting the bottom of a slightly divergent section. The Parshall gauge is calibrated under a piezometric height h measured a few centimetres from the entrance of the converging section. The narrowed or divergent section results in the appearance of a supercritical flow regime flowing over the step. A critical flow depth h_c appears in the throat. The divergent section located downstream of the device makes it possible to transform the supercritical flow into a subcritical flow by means of a hydraulic jump.

There is also the Achour's hydraulic jump flow meter (1989). The apparatus is composed of curved walls constituting the converging part of the device. These surfaces are designed in such a way that any cross section is represented by an isosceles triangle. The converging part of the device therefore constitutes a channel of triangular section with a variable opening angle. It is followed by a section of triangular channel with constant opening angle serving as a transition to the flow and in which the latter becomes critical. The whole assembly thus described has a single bottom of zero slope and a single longitudinal axis. It is thus self-cleaning. The flow passing through the Achour's gauge depends on the depth of the flow at the immediate inlet of the device as well as its geometric characteristics, which is consistent with semi-modular devices.

Another device, a hydraulic jump gauge, also well known is the Venturi flow meter (Bos, 1976; Achour et al., 2003). The Venturi flow meter channel with a flat bottom consists of a channel of rectangular section with horizontal raft of width B which extends over a length equal to at least $1.25\ m + 4h_s$, where h_s is the maximum height of the body of water, of a rectilinear channel section of rectangular section of width b between 10 centimetres and $0.70B$ and which extends over a length $L \geq 1.5hs$. The longitudinal axis of this section must coincide with that of the canal. However, we can tolerate a difference of 2 cm, of a diverging of a length $D = 3(B - b)$ which can, if necessary be reduced by half, i.e. $D = 1.5(B - b)$. The walls of the Venturi meter channel must be smooth and vertical with a tolerance of 0.2%. All dimensions of the device must be observed with a tolerance not exceeding 2 mm.

The flow rate Q given by the Venturi meter depends in particular on two coefficients C_e and C_v. The coefficient C_e depends on the losses due to friction and turbulence and it is a function of h, b and L. It actually depends on the L / b and h / L ratios. Although C_e has been determined for L / b values between 0.20 and 5, the $L / b = 2$ value adopted by some manufacturers appears to be the most useful. The coefficient C_v depends on the velocity of the flow in the upstream channel.

For all the flow rates to be measured by means of the flat-bottom Venturi meter channel, the following conditions must be met: if b/B is greater than 0.35, the height h of the upstream water body must be greater than or at the limit equal to $1.20h_a$, where h_a is the downstream depth of the hydraulic jump, if b / B is less than 0.35, h must be greater than or equal to $1.30h_a$.

The Parshall and Achour gauges, as well as the Venturi flow meter, are so-called semi modular, because the discharge Q is a function of both the upstream depth of the flow and their geometry. Their bottom is flat and their longitudinal axis merges with that of the channel in which they are inserted. This particularity gives these devices a self-cleaning character.

Recent studies have revealed that both broad and thin crested flowmeters without crest height are a serious alternative for measuring flow rates in open channels (Achour, and Amara, 2021; 2022). For these, the theoretical flow rate relationship is very precise and they have many advantages especially broad crested weir designed in a triangular section. Such a section induces excellent precision in the evaluation of both high and low flow rates.

The present study is interested in an extremely simple device which allows the measurement of the flow rate in an open-channel. It simply consists of a rectangular broad-walled U-shaped device with crest height and lateral contraction. The flow then undergoes the dual effect of the lateral and vertical contractions. The ultimate objective in studying this type of device is the theoretical determination of the crossing flow rate relationship that will allow deriving consequently that governing the discharge coefficient. The theoretical determination of the discharge relationship must be done with the requirement to take into account the effect of the approach flow velocity. As the literature indicates, few or even no theoretical previous studies on flow measurement take this effect into account.

The theoretical discharge coefficient relationship will be subjected to an experimental program as intense as it is strict, the aim of which would be to confirm its validity or to correct it if the experimental and theoretical values present some deviations.

MATERIAL AND METHODS

Description of the device and the flow

Fig. 1 shows a schematic perspective representation of the device inserted in a rectangular approach channel of width *B*. The device is in the U shape with broad walls of height h_0 extending over a length *L*. One may perceive along the length *L* a gorge or a groove of width *b* through which the flow passes. This is a central opening contraction.

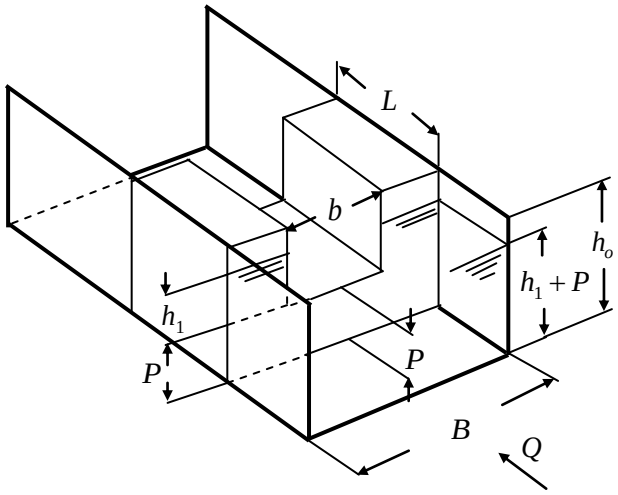

Figure 1: Perspective view of the device placed in a rectangular approach channel of width *B*

The device is removable and it can be placed momentarily in any cross-section of the approach channel to measure the flow rate *Q*. Once the measurement has been taken, the device is then removed. The apparatus is provided with a crest height *P* which is crossed by an upstream flow depth h_1.

The particular case for the configuration represented by Fig. 1 is that for which $P = 0$. The apparatus is then reduced to two prismatic elements placed on either side of the walls of the approach channel.

As clearly shown in Fig. 1, the width *B* of the rectangular approach channel suddenly narrows to a width *b* due to the presence of the device. The flow then undergoes a lateral contraction, the degree of which can be quantified by the ratio $\beta = b / B$. Furthermore, the following relationship gives the physical meaning of the ratio β:

$$\beta = \frac{b}{B} = \frac{b\,h_1}{B\,h_1} = \frac{\text{Contracted section}}{\text{Full section}} \tag{1}$$

It is quite justified to write that $0 < \beta \leq 1$ and that the limiting configuration $\beta = 1$ is reduced to a rectangular broad-crested sill widely cited in the specialized literature (SIA, 1936; Henderson, 1966; Bos, 1976; 1979; Achour et al., 2003). This simple configuration is in use as a standard discharge measuring device and, as such, is clearly described in the British Standard 3680 of 1969. On the other hand, due to the presence of the crest height P (Fig. 1), the flow further undergoes a vertical contraction.

The double effect of lateral and vertical contractions can be expressed by the following dimensionless parameter:

$$\psi = \frac{b\,h_1}{B(h_1 + P)} \tag{2}$$

It is justified to write that the parameter ψ, therefore, represents the ratio of the section located above the crest height to the full section located upstream of the device. After some manipulations, Eq. (2) reduces to:

$$\psi = \frac{\beta}{1 + P^*} \tag{3}$$

where P^* is the relative crest height expressed as:

$$P^* = \frac{P}{h_1} \tag{4}$$

For a given value of β, i.e. for a given installation, it is obvious to write that $\psi \to 0$ when $P^* \to \infty$. This configuration is obtained for large values of the crest height P, i.e. $P \to \infty$, or for low values of the upstream depth h_1, i.e. $h_1 \to 0$. In general, whatever the value taken by the parameters β and P^*, the dimensionless parameter ψ is always less than unity and goes in the range $0 < \psi < 1$.

In the next sections, it will be demonstrated the important role that the dimensionless parameter ψ plays in the flow rate and discharge coefficient relationships.

Fig. 2 schematically shows the longitudinal profile of the flow upstream and inside the device. This profile can be clearly seen in Fig. 3 and what was observed on the thirteen tested devices.

Both in Fig. 2 and Fig. 3, a subcritical flow upstream of the device takes place, while a supercritical flow originates inside the device. The passage between these two natures of the flow is accompanied by the appearance of a control section c-c where the depth of the

flow, denoted h_c, is critical. Fig. 3 illustrates the rectangular test channel and the device in operation as well as the resulting flow confirming that the flow upstream of the device is calm and quiet, showing no appreciable disturbance of the free surface.

The device in operation and the flow produced therein are also shown in Fig. 4 from a downstream view.

On the other hand, the presence of a control section is the prerequisite condition for the correct functioning of the device as a flow measuring means as long as the length *L* is sufficient for the emerging of a control section.

For the case of a rectangular section, the critical depth h_c is written as:

$$h_c = \left(\frac{Q^2}{g\, b^2} \right)^{1/3} \tag{5}$$

where *g* is the acceleration due to gravity.

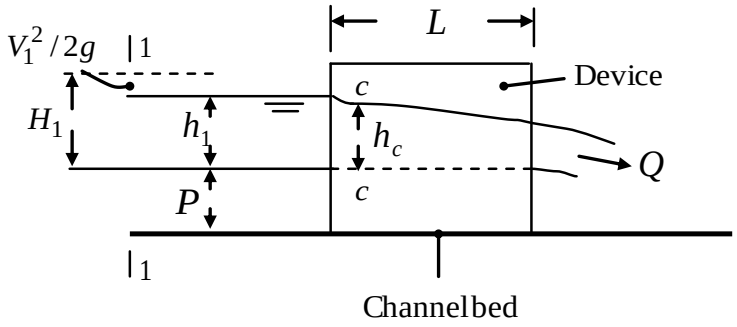

Figure 2: Schematic longitudinal profile of the flow; Subcritical upstream flow in section 1-1; Critical flow depth h_c in section c-c; Supercritical flow inside the device.

Figure 3: Snapshot of longitudinal profile of the flow upstream and inside the device; flow from right to left.

Figure 4: View of the downstream side of the device in operation

The total upstream head above the crest, denoted by H_1 (Fig. 2), is governed by the following relationship:

$$H_1 = h_1 + \frac{V_1^2}{2g} \tag{6}$$

where V_1 denotes the mean flow velocity given by the ratio Q/A_1 where A_1 is the water area in section 1-1 expressed as:

$$A_1 = B(h_1 + P) \tag{7}$$

Thus, Eq. (6) reduces to:

$$H_1 = h_1 + \frac{Q^2}{2g\,B^2\,(h_1 + P)^2} \tag{8}$$

Eq. (8) can be rewritten as:

$$H_1 = \left[1 + \frac{Q^2}{2g\,B^2 h_1\,(h_1 + P)^2}\right] h_1 \tag{9}$$

Eq. (9) takes the following form:

$$H_1 = (1+\delta) h_1 \tag{10}$$

where δ can be interpreted as a kinetic factor governed by the following relationship:

$$\delta = \frac{Q^2}{2g\,B^2 h_1\,(h_1 + P)^2} \tag{11}$$

Eq. (11) simply translates the fact that the kinetic factor δ is such that:

$$\delta = \frac{V_1^2 / 2g}{h_1} \tag{12}$$

In other words, it amounts to writing that $\delta \times h_1 = V_1^2 / 2g$ thus reflecting the fact that the approach velocity head is a fraction δ of the upstream depth h_1.

It is self-evident that the kinetic factor δ is less than unity, varying within the range $0 \le \delta < 1$. It is easy to show that when the flow is critical the value of δ is 1/2. For the case where $\delta \to 0$, the approach flow velocity is then insignificant implying that the total head H_1 can be assimilated to the upstream depth h_1 in accordance with Eq. (10).

It will be seen in an appropriate section that Eq. (11) will play a momentous role in taking into account the approach flow velocity when deriving the theoretical discharge

relationship. It should be emphasized that this effect has been unfairly overlooked in previous studies related to flow metering that could cause appreciable errors when calculating the flow rate. This issue will be highlighted in the section devoted to discharge and discharge coefficient.

Dimensional analysis and discharge coefficient dependency

What is expected from the dimensional analysis is to identify the dimensionless parameters on which the discharge coefficient C_d of the device depends through a qualitative functional relationship. In the current problem which interests the study, one can enumerate ten parameters which influence the phenomenon namely: the discharge Q, the upstream depth h_1, the crest height P, the channel width B, the central opening width b, the crest length L, the acceleration due to gravity g, the density of the flowing liquid ρ, the dynamic viscosity μ of the liquid, and the surface tension σ. These parameters are interrelated by the following functional relationship:

These parameters are interrelated by the following functional relationship:

$$f\left(Q,\rho,g,h_1,B,b,L,P,\mu,\sigma\right)=0 \tag{13}$$

Using Vashy-Buckingham π theorem (Langhaar, 1951), the stage-discharge relationship as function of dimensionless parameters can be derived as follows:

$$Q=g^{1/2}h_1^{3/2}\phi\left(\frac{\rho g^{1/2}h_1^{3/2}}{\mu},\frac{\rho g h_1^2}{\sigma},\frac{h_1}{L},\frac{h_1}{B},\frac{h_1}{b}\frac{h_1}{P}\right) \tag{14}$$

Taking into account the form of the weir equation, one can deduce that ϕ denotes the function symbol expressing the discharge coefficient relationship. one may thus easily recognize the Reynolds number R_e as well as the Weber number W_e represented by the first and the second term in parentheses respectively. Consequently, the discharge coefficient C_d is functionally written as follows:

$$C_d=\phi\left(R_e,W_e,\frac{h_1}{L},\frac{h_1}{B},\frac{h_1}{b},\frac{h_1}{P}\right) \tag{15}$$

It is useful to specify that given the turbulent nature of the flow, the effect of the Reynolds number R_e is not at all significant. Moreover, the effect of the surface tension expressed by the Weber number W_e only appears for low flow rates Q and for small values of the central opening width b, that is to say for a tightened gorge case. On the other hand, the influence of the length L can be neglected provided that the ratio L/h_1 exceeds the lower limit value defining the broad crested criteria. Taking all these considerations into account, Eq. (15) reduces to:

$$C_d = \lambda\left(\frac{h_1}{B}, \frac{h_1}{b}, \frac{h_1}{P}\right) \quad (16)$$

On the other hand, combining the variables h_1 / B and h_1 / b, i.e. by making their ratio, one can form the dimensionless parameter $\beta = b / B$ already expressed by Eq. (1). On the other hand, considering the inverse of the parameter h_1 / P, i.e. $P / h_1 = P^*$, Eq. (16) can be then written in its following final form:

$$C_d = \lambda\left(\beta, P^*\right) \quad (17)$$

It is thus demonstrated that the discharge coefficient C_d of the considered device depends on both β and P^*. It is useful to recall that these two dimensionless parameters have been grouped together in the single variable ψ expressed by Eq. (3).

The functional relationship λ will be theoretically defined in the next sections through the use of both momentum and energy equations.

Theoretical relative depth and relative total head relationships

The relative depth, noted h_1^*, is the ratio of the upstream depth h_1 to the critical depth h_c inside the device in section c-c (Fig. 2). Thereby:

$$h_1^* = \frac{h_1}{h_c} \quad (18)$$

It was found that the relative depth h_1^* could be expressed by a relationship derived from the application of the momentum equation. It is worth noting that the momentum equation applies while assuming some simplifying assumptions which considerably simplify the problem presently handled. These hypotheses result from the fact that hydraulic phenomena occurring in the subject tackled by the study are not yet mastered from a theoretical point of view. Recent studies have clearly shown that these simplifying assumptions are fully justified having no real impact on the final experimental results (Achour and Amara, 2021; 2022). These are namely: The pressure distribution is assumed to be hydrostatic in any section of the flow, outside or inside the device; in the selected sections 1-1 and c-c (Fig. 2), the flow velocity is assumed to be uniform; the friction loss between the selected sections, separated by a short distance, is assumed to be insignificant, and both effects of air resistance and of the streamlines curvature are neglected.

The momentum theorem states that the variation of the quantity ρQV is equal to the algebraic sum of all the external forces acting on the selected sections, after having projected them on a longitudinal axis. It is simple to consider the direction of this axis as being that of the flow.

Let us define the external forces that act on the selected sections 1-1 of water area A_1 and c-c of water area A_c as: F_1 the pressure force acting on the section 1-1, F_c the pressure force acting on the selected critical section c-c, and F_R the reaction force acting on the upstream side of the device. The hydrostatic pressure forces F_1 and F_c can be respectively written as:

$$F_1 = \frac{1}{2}\rho g B\left(h_1 + P\right)^2 \tag{19}$$

$$F_c = \frac{1}{2}\rho g b h_c^2 \tag{20}$$

while F_R is governed by the following relationship:

$$F_R = \rho g \overline{h_R} A_R \tag{21}$$

where $\overline{h_R}$ is the depth at the centroid of the upstream cross-section area A_R of the device on which the reaction force F_R is acting. Note that the vertical distance $\overline{h_R}$ must be counted from the free surface flow. It is easy to show that:

$$\overline{h_R} = \frac{1}{2}\frac{B(h_1+P)^2 - b h_1^2}{A_R} \tag{22}$$

where A_R is as:

$$A_R = B(h_1 + P) - b h_1 \tag{23}$$

After projecting the three acting forces on the longitudinal axis, the momentum equation becomes:

$$\rho Q\left(V_c - V_1\right) = F_1 - F_c - F_R \tag{24}$$

V_c denotes the mean velocity at the critical cross-section c-c (Fig. 2). Taking into account Eqs. (19), (20), (21), (15), along with considering that $V_c = Q/A_c = Q/(b\,h_c)$ and $V_1 = Q/A_1 = Q/[B(h_1+P)]$, Eq. (24) reduces to:

$$h_1^{*3} - 3h_1^* + \frac{2\beta}{1+P^*} = 0 \tag{25}$$

Let us recall that the dimensionless parameters β and P^* are defined by Eqs. (1) and (4) respectively and which are both grouped in the same parameter ψ according to Eq. (3). Therefore, Eq. (25) can be rewritten as follows:

$$h_1^{*3} - 3h_1^* + 2\psi = 0 \tag{26}$$

Thus, according to Eq. (26), the relative depth h_1^* depends solely on the dimensionless compound parameter ψ.

Eq. (26) is a third degree equation without second order term. It admits three real roots, only one of which satisfies the physical condition $h_1^* > 1$, since $h_1 > h_c$. Using the method described by Spiegel (1974), the only solution of Eq. (26) which must be retained is:

$$h_1^* = 2\cos\left[\frac{1}{3}\cos^{-1}(-\psi)\right] \tag{27}$$

As with the relative upstream depth h_1^*, the relative upstream total head H_1^* is defined as the ratio of the total head H_1 in the section 1-1 (Fig. 2) to the critical depth h_c in the section c-c inside the device, i.e.:

$$H_1^* = \frac{H_1}{h_c} \tag{28}$$

On the other hand, dividing both sides of Eq. (8) by h_c yields:

$$H_1^* = h_1^* + \frac{Q^2}{2gB^2(h_1+P)^2 h_c} \tag{29}$$

Eliminating the discharge Q between Eqs. (5) and (29) results in:

$$H_1^* = h_1^* + \frac{g b^2 h_c^3}{2gB^2(h_1+P)^2 h_c} \tag{30}$$

After some simplifications and rearrangements, Eq. (30) reduces to:

$$H_1^* = h_1^* + \frac{\psi^2}{2h_1^{*2}} \tag{31}$$

With regard to Eqs. (27) and (31), it is obvious to conclude that the relative upstream total head H_1^* is exclusively dependent on the dimensionless compound parameter ψ. Inserting Eq. (27) into Eq. (31) results in:

$$H_1^* = 2\cos\left[\frac{1}{3}\cos^{-1}(-\psi)\right] + \frac{\psi^2}{8\cos^2\left[\frac{1}{3}\cos^{-1}(-\psi)\right]} \tag{32}$$

Eq. (32) is valid for $0 < \psi < 1$. For a designated installation characterized by a given value of both β and P^*, i.e. for a specified parameter ψ, Eq. (32) allows explicitly calculating the relative total head H_1^*. However, the form of Eq. (32) is somewhat complicated and inappropriate, not facilitating the simplicity of the theoretical equations expected during the remainder of the study. Therefore, it is recommended to use in place of Eq. (32) the following explicit relationship, simple and useful, resulting from an in-depth correlation analysis:

$$H_1^{*\,-1} = \frac{h_c}{H_1} = \zeta(\psi) = 0.103\psi + 0.5789 \tag{33}$$

Eq. (33) is valid in the wide range $0.1 \le \psi \le 0.65$, thus encompassing most of the practical cases. It was obtained with the following quality coefficient of determination $R^2 = 0.9991$. In the above stated range of the dimensionless parameter ψ, the maximum relative deviation caused by the use of the approximate Eq. (33) on the $H_1^{*\,-1}$ calculation is only 0.16%, observed for the greatest considered value of ψ, i.e. $\psi = 0.65$. The simple form of Eq. (33) will be very useful for the remainder of the theoretical development which is not the case by making use of the original Eq. (32).

Discharge and discharge coefficient relationships

Combining Eqs. (5), (10) and (33) yields:

$$h_c = \left(\frac{Q^2}{gb^2}\right)^{1/3} = (1+\delta)\zeta(\psi)h_1 \tag{34}$$

The following result can then be easily obtained:

$$Q^2 = gb^2(1+\delta)^3\zeta^3 h_1^3 \tag{35}$$

Elimination Q^2 between Eqs. (11) and (35) and rearranging results in:

$$\delta = \frac{1}{2}\xi^2(1+\delta)^3 \tag{36}$$

where the function ξ is governed by the following relationship depending solely on ψ:

$$\xi = \psi\,\zeta^{3/2} \tag{37}$$

Eq. (36) can be rewritten as:

$$\frac{(1+\delta)^3}{\delta} = \frac{2}{\xi^2} \tag{38}$$

It is quite obvious that the kinetic factor δ depends only on the parameter ψ. In the whole range $0 < \psi < 1$, it is easy to observe that the kinetic factor δ is always less than unity. This allows writing that $(1+\delta)^3 \approx (1+3\delta)$ resulting from the first order Taylor series expansion. Inserting this convenient result into Eq. (38) results in:

$$\delta = \frac{\xi^2}{2-3\xi^2} \tag{39}$$

Eq. (39) along with Eq. (37) allows explicitly computing the kinetic factor δ that reflects the effect of the approach flow velocity, depending solely on the dimensionless parameter ψ. Table 1 groups together the calculated values of the kinetic factor δ for a given value of the relative crest height P^*. As it can be seen, the effect of the approach flow velocity cannot always be neglected, in particular for large values of ψ.

Table 1: Values of the kinetic factor δ for some values of the parameter ψ according to Eq. (39) along with Eq. (37)

P^*	β	ψ	ξ	δ	$(1+\delta)^{3/2}$
0.40	0.1	0.07142857	0.032063	0.00051481	1.00077232
	0.15	0.10714286	0.04854788	0.00118263	1.00177447
	0.2	0.14285714	0.06533689	0.00214821	1.00322405
	0.25	0.17857143	0.08243145	0.00343246	1.0051531
	0.3	0.21428571	0.09983296	0.00505894	1.007598
	0.35	0.25	0.11754282	0.00705435	1.01060017
	0.4	0.28571429	0.13556241	0.00944905	1.01420701
	0.45	0.32142857	0.15389312	0.01227771	1.01847297
	0.5	0.35714286	0.17253634	0.0155801	1.02346094
	0.55	0.39285714	0.19149344	0.01940207	1.02924382
	0.6	0.42857143	0.21076578	0.02379676	1.03590667
	0.65	0.46428571	0.23035473	0.02882606	1.04354921

As an illustrative example that allows affirming that the effect of the approach flow velocity cannot be neglected in all cases, let us consider for this the value $\beta = 0.50$. According to table 1, the kinetic factor δ is such that $\delta = 0.0155801$. Let us then calculate

the quantity $(1+\delta)^{3/2}$ involved in Eq. (35) expressing the flow rate Q. The calculation gives:

$$(1+\delta)^{3/2} = 1.02346094$$

When taking for example the case corresponding to $\beta = 0.50$ and $P^* = 0.40$, if one were to neglect the approach flow velocity, more than 2.3% of error would be then committed in the calculation of the flow rate *Q*. This result would be undesirable in certain practical cases that would require more precision.

Eq. (39) allows writing that:

$$(1+\delta)^{3/2} = \left(\frac{1-\xi^2}{1-\frac{3}{2}\xi^2} \right)^{3/2} \tag{40}$$

Inserting Eq. (40) into Eq. (35) yields:

$$Q = \sqrt{g}\, b \left(\frac{1-\xi^2}{1-\frac{3}{2}\xi^2} \right)^{3/2} \zeta^{3/2} h_1^{3/2} \tag{41}$$

Eq. (41) can be rewritten as:

$$Q_{Th} = \frac{1}{\sqrt{2}} \sqrt{2g}\, b \left(\frac{1-\xi^2}{1-\frac{3}{2}\xi^2} \right)^{3/2} \zeta^{3/2} h_1^{3/2} \tag{42}$$

The subscript « *Th* » denotes « Theoretical ».

It is useful to remember that the functions ζ and ξ are governed by Eqs. (33) and (37) respectively. Eq. (42) is the first form of the flow rate *Q* passing through the device. Eq. (42) clearly shows that the flow rate is a function both of the geometric characteristics of the device and of the upstream depth of the flow. It therefore perfectly conforms to the so-called semi-modular devices.

Eq. (42) can be written in the following reduced form like that of rectangular weirs:

$$Q = C_{d,1} \sqrt{2g}\, b\, h_1^{3/2} \tag{43}$$

where the discharge coefficient $C_{d,1}$ is as follows depending solely on the dimensionless parameter ψ:

$$C_{d,1} = \frac{\zeta^{3/2}}{\sqrt{2}} \left(\frac{1-\xi^2}{1-\frac{3}{2}\xi^2} \right)^{3/2} \tag{44}$$

It is the theoretical relationship of the discharge coefficient of the considered device, taking into account the effect of the approach flow velocity reflected by the quantity in parentheses. It is this relationship that will have to be compared with experimental results.

On the other hand, rearranging Eq. (42) results in the following second formulation of the discharge Q:

$$Q_{Th} = \frac{1}{\sqrt{2}} \sqrt{2g}\, B \left(\frac{1-\xi^2}{1-\frac{3}{2}\xi^2} \right)^{3/2} \xi\, h_1^{3/2} \tag{45}$$

Eq. (45) can be written in the form of Eq. (43) yielding:

$$Q = C_{d,2} \sqrt{2g}\, B\, h_1^{3/2} \tag{46}$$

where the discharge coefficient $C_{d,2}$ is governed by the following relationship:

$$C_{d,2} = \frac{\xi}{\sqrt{2}} \left(\frac{1-\xi^2}{1-\frac{3}{2}\xi^2} \right)^{3/2} \tag{47}$$

It is worth noting that Eq. (42) or Eq. (45) governing the flow rate is conforms to that of a semi-modular apparatus since Q is given as a function of the geometric characteristic of the device represented by the width b of the contraction central opening and of the upstream depth h_1 as well.

Experimental validation

The main objective of this part of the study is the experimental verification of Eq. (44) governing the discharge coefficient C_d of the device. It could be that Eq. (44) either validated in its current form or corrected if deviations between the experimental and theoretical values are observed. If the validity of Eq. (44) would be confirmed, then Eq. (42) which governs the flow rate Q would also be.

To carry out the experimental program implemented, no less than thirteen devices with different geometric characteristics were designed and carefully tested. They were designed in transparent Plexiglass.

The channel used for the tests is a rectangular channel 12 meters long, 0.293 meter wide and 0.485 meter deep the overall view of which is shown in Fig. 5.

Figure 5: Overview of the rectangular test channel.

The channel is supplied by a pump providing a maximum discharge Q slightly above 30 l/s. The entire hydraulic system operates in a closed circuit to ensure a permanent flow.

Table 2 shows the data relating to the thirteen tested devices, more specifically their geometric characteristics, as well as the ranges of the flow rate Q used for each of them.

It also indicates the ranges of values of the measured upstream depths h_1 corresponding to each flow rate range. For all the tests carried out, the length L of the tested devices was kept constant equal to L = 0.25 m, which was sufficient for the appearance of the control section inside the gorge.

As can therefore be seen from Table 2, no less than 240 measurement points of the pair of parameters (Q, h_1) were collected and the values of which are fully reported in the tables 3 to 15 in appendix. It is a sufficiently representative sample to perform a reliable experimental analysis.

Table 2: Geometric characteristics, range of flow rate and upstream depth used during the thirteen tested devices

$\beta = b/B$	Crest height P (cm)	Number of Measurements	Discharge range (l/s)	Range of upstream depth (cm)
0.5017	10	18	$2.11 \leq Q \leq 26.68$	$4.630 \leq h_1 \leq 23.972$
0.5017	8	19	$1.48 \leq Q \leq 23.57$	$3.662 \leq h_1 \leq 21.990$
0.5017	6	18	$2.00 \leq Q \leq 23.22$	$4.412 \leq h_1 \leq 21.620$
0.4505	8	19	$1.63 \leq Q \leq 24.67$	$4.258 \leq h_1 \leq 24.698$
0.4505	6	19	$2.03 \leq Q \leq 21.53$	$4.800 \leq h_1 \leq 22.324$
0.3993	10	17	$2.42 \leq Q \leq 22.50$	$5.908 \leq h_1 \leq 25.332$
0.3993	8	20	$1.68 \leq Q \leq 24.96$	$4.642 \leq h_1 \leq 27.020$
0.3993	6	17	$1.92 \leq Q \leq 19.76$	$5.028 \leq h_1 \leq 23.074$
0.3481	8	18	$2.06 \leq Q \leq 18.86$	$5.834 \leq h_1 \leq 24.834$
0.3481	6	19	$2.93 \leq Q \leq 23.72$	$7.300 \leq h_1 \leq 28.744$
0.3003	10	18	$2.72 \leq Q \leq 18.40$	$7.764 \leq h_1 \leq 27.204$
0.3003	8	20	$2.81 \leq Q \leq 18.46$	$7.892 \leq h_1 \leq 27.202$
0.3003	6	18	$1.43 \leq Q \leq 17.87$	$5.056 \leq h_1 \leq 26.534$

As the study focuses on the problem of a flowmeter and mainly the validation of the discharge coefficient relationship, it is therefore recommended to measure the hydraulic parameters involved with irreproachable precision. As will be seen later, the hydraulic parameters which are involved in the experimental discharge coefficient are both the flow rate Q and the upstream depth h_1. To meet this requirement, an ultrasonic flowmeter, with an accuracy of around 0.1 to 0.2 l/s, was used for the measurement of the flow rate Q. As for the upstream depth h_1, it was measured using a double-precision Vernier point-gauge graduated to 1/10th in order to minimize reading errors on the depth causing an absolute error of 0.02 mm only.

For each test, i.e. for each pair of measured values (Q_{Exp} , h_1), the experimental discharge coefficient $C_{d,Exp}$ of the tested device is calculated in accordance with Eq. (43). That is to say:

$$C_{d,Exp} = \frac{Q_{Exp}}{\sqrt{2g}\, b\, h_1^{3/2}} \tag{48}$$

where the subscript "*Exp*" denotes "Experimental". Eq. (48) was used to calculate every experimental discharge coefficient of the same device corresponding to all the flow rates belonging to the tested series. The corresponding theoretical discharge coefficients $C_{d,Th}$ were calculated according to Eq. (44) in which fully parameters are known, especially the two functions ζ and ξ.

At the end of the calculations, 240 experimental discharge coefficients $C_{d,Exp}$ and as many theoretical discharge coefficients $C_{d,Th}$ were obtained. The 240 values of $C_{d,Exp}$ and $C_{d,Th}$ were compared and their variation plotted in Fig. 6.

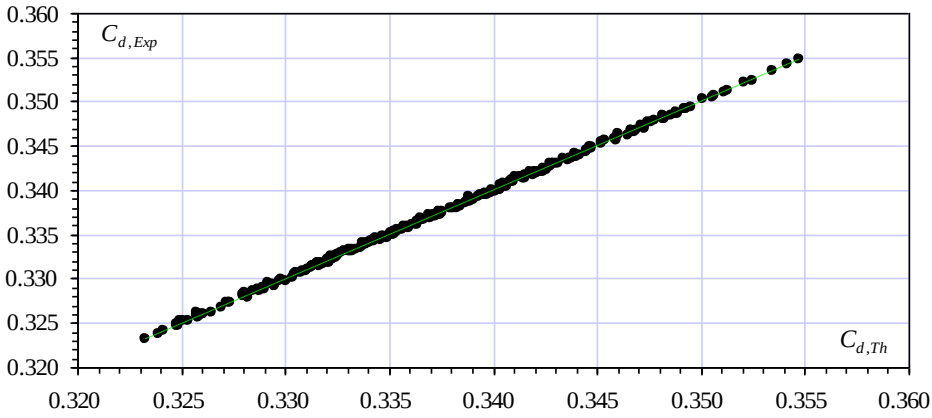

Figure 6: Variation of experimental discharge coefficient $C_{d,Exp}$ versus theoretical discharge coefficient $C_{d,Th}$ computed according to Eq. (44). (- - -) Trend line

Through Fig. 6, one may observe with satisfaction an almost perfect alignment of the experimental and theoretical values of the discharge coefficient on a straight line. Experience thus proves the validity of the theory, in this instance Eq. (44) governing the theoretical discharge coefficient, even though no calibration parameter was employed. The use of linear least-squares fitting method involving experimental and theoretical data gave the following trend line relationship:

$$C_{d,Exp} = 0.9999\, C_{d,Th} \tag{49}$$

Eq. (49) was obtained with a coefficient of determination $R^2 = 0.9995$. Eq. (49) clearly shows that the ratio $C_{d,Exp} / C_{d,Th}$ is extremely close to unity, which allows concluding that the theoretical Eq. (44) does not need any correction. It can be used with confidence to estimate with a great precision the discharge coefficient of the device. Thus, this is obviously also the case for the theoretical relationship (42) governing the flow rate Q.

CONCLUSION

The semi-modular rectangular cross-section flow meter with a lateral contraction has been rigorously subjected to theoretical and experimental investigations. The theoretical development had the dual ambition of deriving the relationship that governs the flow rate Q and consequently that of the discharge coefficient C_d while taking into account the effect of the approach flow velocity. As the literature has shown, this effect has always been overlooked in previous studies on flow metering in open channels.

This dual objective was achieved with ease and rigor by making use of the momentum theorem and the energy equation as well. This choice was motivated by the fact that the momentum theorem and the energy equation have unmistakably proved their worth in recent studies carried out by the authors. This is how the theoretical Eqs. (42) and (44) which govern the flow Q and the discharge coefficient C_d respectively have been successfully established. The flow rate relationship was in accordance with semi-modular devices since Q depends both on the geometric characteristics of the device as well as on the upstream depth of the flow.

Eq. (44) that governs the discharge coefficient C_d contains two functions ζ and ξ depending exclusively on the dimensional parameter ψ defined as being the contraction rate of the inflow cross-section. It reflects at the same time the double effect of the lateral and vertical contractions of the flow.

The study continued with an experimental program that was both intense and exacting. The ultimate goal was to corroborate or possibly correct the theoretical Eq. (44) governing the discharge coefficient C_d, knowing that if it would be verified then Eq. (42) which governs the flow rate Q would also be.

For this, no less than thirteen devices with different geometric characteristics have been designed and tested in an appropriate hydraulic installation. Each of the devices was placed in the test channel and underwent a series of values of the flow rate Q which generated as many values of the upstream depth h_1. In total, 240 experimental points for the couple (Q, h_1) were collected for the thirteen devices involved during the tests. It is an extremely representative sample which would allow a reliable experimental analysis.

The experimental values of the discharge coefficient calculated according to Eq. (48) were compared with those of the theoretical discharge coefficient resulting from Eq. (44). It was then observed with complete satisfaction an excellent agreement between them as clearly shown in Fig. (6). This confirmed on one hand the correctness of the theoretical approach and that on the other hand the simplifying assumptions on which it was based were founded since they had no effect on the quality of the results.

Ultimately, the use of linear least-squares fitting method involving experimental and theoretical data showed, with an excellent coefficient of determination, that the ratio $C_{d,Exp} / C_{d,Th}$ ratio was very close to unity. This high-quality result allowed affirming that the theoretical Eq. (44) governing the discharge coefficient did not need any correction and, therefore, can be used with complete confidence in its current form.

It is desirable to end this conclusion by stating some advantages and disadvantages of the apparatus advocated in the present study. The device has many advantages namely : it is simple in design; it can be placed in any section of the canal as it is removable; it allows easily calculating the flow rate carried by the channel by an extremely reliable theoretical relationship which only requires knowing the geometric characteristic of the device as well as the upstream depth of the flow; the theoretical flow rate relationship does not require any correction and the device does not need to be calibrated.

On the other hand, two main disadvantages should be noted. The first relates to the rectangular shape of the device. It is well known in the field of flow measurement that the rectangular section does not allow good precision in the gauging of low flow rates, unlike the triangular section. This imprecision is mainly due to the reading of shallow depths and it is therefore recommended to measure them with a high precision device such as that used in the present study in order to minimize reading errors. The second disadvantage is that the apparatus is provided with a crest height *P* which acts as a barrier resulting in the accumulation of solid deposits. Due to the presence of the crest height *P*, the device is unfortunately not self-cleaning requiring periodic cleaning.

REFERENCES

ACHOUR B. (1989). Débitmètre à ressaut en canal de section droite triangulaire sans seuil, Jump flow meter in a triangular cross-section without weir, Journal of Hydraulic Research, Vol. 27, Issue 2, pp. 205-214, In French.

ACHOUR B., BOUZIANE M.T., NEBBAR M.L. (2003). Débitmètre triangulaire à paroi épaisse dans un canal rectangulaire, Triangular broad walled flowmeter in a rectangular channel, Larhyss Journal, No 2, pp. 7-43, In French.

ACHOUR B., AMARA L. (2021). Discharge measurement in a rectangular open-channel using a sharp-edged width constriction - theory and experimental validation, Larhyss Journal, No 45, pp. 141-163.

ACHOUR B., AMARA L. (2022). Flow measurement using a triangular broad crested weir - theory and experimental validation, Flow Measurement and Instrumentation, Vol. 83, 102088, pp. 1-10.

BAZIN H. (1898). Expériences nouvelles sur l'écoulement en déversoir, New experiments on weir flow, Ed. Dunod, Paris, In French.

BOS M.G. (1976). Discharge measurement structures, hydraulic laboratory, Wageningen, The Netherlands, Report 4, May.

BOS M.G. (1989). Discharge Measurement Structures, third Ed., Publication 20, International Institute for Land Reclamation and Improvement, Wageningen, The Netherlands.

BOUSSINESQ J.M. (1877). Théorie des eaux courantes, Mémoires présentés par divers savants, Académie des Sciences de France, Theory of running waters, Memoirs presented by various scientists, French Academy of Sciences, Vol. 23, In French.

British Standard (1969). MEASUREMENT OF LIQUID FLOW OPEN CHANNELS – MEASURING INSTRUMENTS AND EQUIPMENTS, HTTPS://DOI.ORG/10.3403/BS3680

DE COURSEY D.E., BLANCHARD B.J. (1970). Flow analysis over large triangular weir, Proceeding American Society of Civil Engineers, ASCE, Journal of Hydraulics Division, Vol. 96, HY7, pp. 1435-1454.

HAGER W.H. (1986). Discharge Measurement Structures, Communication 1, Département de Génie Civil, Ecole Polytechnique Fédérale de Lausanne, Suisse, Department of Civil Engineering, Federal Polytechnic School of Lausanne, Switzerland.

HENDERSON F.M. (1966). Open Channel Flow, The McMillan Company, New York, N.Y, USA, 522p.

KINDSVATER C.E., CARTER R.W. (1957). Discharge characteristics of rectangular thin-plate weirs, Proceeding American Society of Civil Engineers, ASCE, Journal of Hydraulics Division, Vol. 83, HY6, pp.1453/1-6.

LANGHAAR H.L. (1951). Dimensional Analysis and Theory of Models, John Wiley and Son Ltd, 1st Edition, 166p.

LENZ A.T. (1943). Viscosity and surface tension effects on V-notch coefficients, Transactions American Society of Civil Engineers, ASCE, Vol. 108, pp. 759-781.

RAMPONI F. (1949). Sulle forme di imbocco dei canali e delle opere di scarico superficiali, L'Energia Electrica, Vol. 26, pp. 453-460.

REHBOCK T. (1929). Wassermessung mit scharfkantigen Ueberfaellen, Zeitschrift VdI, Vol. 73, pp. 817-823.

SARGINSON E.J. (1972). The influence of surface tension on weir flow, Journal of Hydraulic Research, Vol. 10, Issue 4, pp. 431- 446.

SARGINSON E.J. (1972). The influence of surface tension on weir flow, Journal of Hydraulic Research, Vol. 10, Issue 4, pp. 431-443.

SIA (1926). Contribution à l'étude des méthodes de jaugeages, Contribution to the study of gauging methods, Bull. 18, Schw., Bureau Wasserfoschung, Bern, 1926, In French.

SPIEGEL M.R. (1974). Mathematical Handbook of Formulas and Tables, 20th Edition, McGraw Hill Inc, New York, USA.

APPENDIX

Table 3: Experimental values of h_1 and Q for the device defined by b = 0.147 m, P = 0.10 m, B = 0.293 m

Run	h_1(m)	Q_{Exp} ($m^3.s^{-1}$)
1		
2	0.0463	0.002115
3	0.09542	0.00644
4	0.10986	0.007995
5	0.11901	0.00905
6	0.12902	0.01025
7	0.13788	0.011367
8	0.14786	0.01265
9	0.15674	0.01385
10	0.16466	0.01494
11	0.17476	0.01638
12	0.18346	0.01766
13	0.1912	0.01882
14	0.20136	0.0204
15	0.20832	0.0215
16	0.21544	0.02264
17	0.2248	0.02415
18	0.23316	0.02555
19	0.23972	0.02668

Table 4: Experimental values of h_1 and Q for the device defined by b = 0.147 m, P = 0.08 m, B = 0.293 m

Run	h_1 (m)	Q_{Exp} ($m^3.s^{-1}$)
1	0.03662	0.001487
2	0.04432	0.001994
3	0.06076	0.00324
4	0.0721	0.004215
5	0.08564	0.005498
6	0.10076	0.00707
7	0.109	0.00798
8	0.12104	0.00938
9	0.13256	0.010797
10	0.1425	0.01208
11	0.1548	0.01373
12	0.16186	0.0147
13	0.1704	0.01592
14	0.17986	0.01729
15	0.18698	0.01836
16	0.19706	0.0199
17	0.2048	0.021137
18	0.21236	0.02234
19	0.2199	0.02357

Table 5: Experimental values of h_1 and Q for the device defined by b = 0.147 m, P = 0.06 m, B = 0.293 m

Run	h_1 (m)	Q_{Exp} ($m^3.s^{-1}$)
1	0.04412	0.002002
2	0.0543	0.002755
3	0.0664	0.00376
4	0.0823	0.00524
5	0.09366	0.0064
6	0.09948	0.00702
7	0.10654	0.007805
8	0.11622	0.00893
9	0.12494	0.00998
10	0.13412	0.01113
11	0.14524	0.012585
12	0.15878	0.01444
13	0.16682	0.01558
14	0.1767	0.01703
15	0.18178	0.01778
16	0.19536	0.01987
17	0.2072	0.02175
18	0.2162	0.02322

Table 6: Experimental values of h_1 and Q for the device defined by b = 0.132 m, P = 0.08 m, B = 0.293 m

Run	h_1 (m)	Q_{Exp} ($m^3.s^{-1}$)
1	0.04258	0.001673
2	0.05792	0.002685
3	0.0718	0.00373
4	0.0849	0.00483
5	0.0987	0.00609
6	0.11106	0.0073
7	0.11986	0.00821
8	0.13274	0.0096
9	0.14228	0.01068
10	0.1534	0.012
11	0.16412	0.0133
12	0.17118	0.0142
13	0.18568	0.0161
14	0.19708	0.01764
15	0.2086	0.01925
16	0.21904	0.02072
17	0.22948	0.02225
18	0.2365	0.0233
19	0.24698	0.0249

Table 7: Experimental values of h_1 and Q for the device defined by b = 0.132 m, P = 0.06 m, B = 0.293 m

Run	h_1 (m)	Q_{Exp} ($m^3.s^{-1}$)
1	0.048	0.00203
2	0.05196	0.002295
3	0.06288	0.003078
4	0.08324	0.00474
5	0.09348	0.00566
6	0.10924	0.0072
7	0.12132	0.00845
8	0.13082	0.00949
9	0.14044	0.01058
10	0.14612	0.01125
11	0.15456	0.01227
12	0.16604	0.0137
13	0.1785	0.01529
14	0.18498	0.01615
15	0.19306	0.01725
16	0.19988	0.0182
17	0.2076	0.01927
18	0.21452	0.02025
19	0.22324	0.02153

Table 8: Experimental values of h_1 and Q for the device defined by b = 0.117 m, P = 0.10 m, B = 0.293 m

Run	h_1 (m)	Q_{Exp} ($m^3.s^{-1}$)
1	0.05908	0.00242
2	0.10974	0.006245
3	0.1202	0.00718
4	0.12902	0.008
5	0.14092	0.00916
6	0.15022	0.0101
7	0.1577	0.01088
8	0.16368	0.01153
9	0.1735	0.0126
10	0.18382	0.01376
11	0.19038	0.01452
12	0.20072	0.01575
13	0.20998	0.01686
14	0.21878	0.01796
15	0.23034	0.01945
16	0.2421	0.02097
17	0.25332	0.0225

Table 9: Experimental values of h_1 and Q for the device defined by b = 0.117 m, P = 0.08 m, B = 0.293 m

Run	h_1 (m)	Q_{Exp} ($m^3.s^{-1}$)
1	0.04642	0.001684
2	0.05914	0.00244
3	0.10884	0.00621
4	0.12532	0.00771
5	0.1384	0.00897
6	0.14928	0.01008
7	0.1626	0.01148
8	0.17556	0.01293
9	0.18898	0.01445
10	0.20246	0.01606
11	0.20902	0.01686
12	0.21588	0.01772
13	0.22328	0.01867
14	0.22948	0.01944
15	0.23568	0.02028
16	0.24244	0.02115
17	0.24884	0.02201
18	0.25558	0.02292
19	0.26172	0.02377
20	0.2702	0.02496

Table 10: Experimental values of h_1 and Q for the device defined by b = 0.117 m, P = 0.06 m, B = 0.293 m

Run	h_1 (m)	Q_{Exp} ($m^3.s^{-1}$)
1	0.05028	0.00192
2	0.07726	0.00371
3	0.0863	0.00439
4	0.10596	0.00602
5	0.1157	0.00688
6	0.12402	0.00765
7	0.13758	0.00897
8	0.1441	0.00963
9	0.15408	0.01067
10	0.16426	0.01178
11	0.17112	0.01252
12	0.18132	0.01369
13	0.18958	0.01465
14	0.19954	0.01584
15	0.2101	0.01715
16	0.2202	0.0184
17	0.23074	0.01976

Table 11: Experimental values of h_1 and Q for the device defined by b = 0.102 m, P = 0.08 m, B = 0.293 m

Run	h_1 (m)	Q_{Exp} ($m^3.s^{-1}$)
1	0.05834	0.002067
2	0.06214	0.002276
3	0.08306	0.00355
4	0.09474	0.00434
5	0.11632	0.00593
6	0.12266	0.00644
7	0.1319	0.007195
8	0.1399	0.00787
9	0.14826	0.00859
10	0.16436	0.01006
11	0.17394	0.01097
12	0.18298	0.01185
13	0.19564	0.01312
14	0.20824	0.01443
15	0.21934	0.01562
16	0.22912	0.016704
17	0.2378	0.01766
18	0.24834	0.01886

Table 12: Experimental values of h_1 and Q for the device defined by b = 0.102 m, P = 0.06 m, B = 0.293 m

Run	h_1 (m)	Q_{Exp} ($m^3.s^{-1}$)
1	0.073	0.002935
2	0.08562	0.003745
3	0.09738	0.00456
4	0.11028	0.00551
5	0.1254	0.00671
6	0.13848	0.0078
7	0.15236	0.00902
8	0.16692	0.01037
9	0.17882	0.01152
10	0.20098	0.01376
11	0.20876	0.01458
12	0.2196	0.01575
13	0.229	0.01678
14	0.23718	0.0177
15	0.24946	0.01912
16	0.26044	0.02042
17	0.26814	0.02132
18	0.27718	0.02242
19	0.28744	0.02372

Table 13: Experimental values of h_1 and Q for the device defined by b = 0.088 m, P = 0.10 m, B = 0.293 m

Run	h_1 (m)	Q_{Exp} ($m^3.s^{-1}$)
1	0.07764	0.002725
2	0.08758	0.003275
3	0.10814	0.00452
4	0.13258	0.00616
5	0.14586	0.00713
6	0.15866	0.008101
7	0.16576	0.00865
8	0.17596	0.00947
9	0.18346	0.0101
10	0.19088	0.01072
11	0.20066	0.01158
12	0.21186	0.01257
13	0.22566	0.01384
14	0.24266	0.01545
15	0.24932	0.0161
16	0.25616	0.01677
17	0.2641	0.01757
18	0.27204	0.0184

Table 14: Experimental values of h_1 and Q for the device defined by b = 0.088 m, P = 0.08 m, B = 0.293 m

Run	h_1 (m)	Q_{Exp} ($m^3.s^{-1}$)
1	0.07892	0.00281
2	0.08596	0.0032
3	0.09446	0.003691
4	0.10628	0.00442
5	0.11874	0.00523
6	0.1282	0.00588
7	0.14108	0.0068
8	0.14796	0.00732
9	0.163	0.00848
10	0.17566	0.0095
11	0.18276	0.01009
12	0.19116	0.010798
13	0.2018	0.01173
14	0.20858	0.01234
15	0.21848	0.01324
16	0.22906	0.01423
17	0.23954	0.01523
18	0.24978	0.01622
19	0.26028	0.01726
20	0.27202	0.01846

Table 15: Experimental values of h_1 and Q for the device defined by b = 0.088 m, P = 0.06 m, B = 0.293 m

Run	h_1 (m)	Q_{Exp} ($m^3.s^{-1}$)
1	0.05056	0.001435
2	0.05708	0.001726
3	0.06724	0.002215
4	0.07558	0.0026465
5	0.08714	0.00329
6	0.09804	0.003936
7	0.13988	0.00676
8	0.1515	0.00763
9	0.16204	0.00845
10	0.17156	0.009228
11	0.18216	0.0101
12	0.1972	0.0114
13	0.2072	0.01228
14	0.22044	0.0135
15	0.23086	0.01446
16	0.2445	0.01577
17	0.2561	0.01692
18	0.26534	0.01787